Chemical Engineering Journal 146 (2009) 128–135

Contents lists available at ScienceDirect

Chemical Engineering Journal

journal homepage: www.elsevier.com/locate/cej

Design of a CO preferential oxidation reactor for PEFC systems: A modelling approach

F. Cipitì*, V. Recupero

Institute CNR-ITAE, Via S. Lucia sopra Contesse n. 5, 98126 S. Lucia, Messina 98126, Italy

ARTICLE INFO

Article history:
Received 11 January 2008
Received in revised form 4 September 2008
Accepted 5 September 2008

Keywords:
Fuel processor
CO preferential oxidation
Hydrogen oxidation
Hydrogen production
Two-dimensional catalytic modeling

ABSTRACT

This paper presents a two-dimensional model of a preferential oxidation (PROX) reactor to be used in a beta 5 kWe hydrogen generator (HYGen II), to integrate with Polymer Electrolyte Fuel Cells (PEFCs). PROX reactors require careful temperature control systems, in order to enhance optimization and control of the unit. The model concerns chemical kinetics and heat/mass transfer phenomena occurring in the reactor. Aim of the model is to investigate the effects of the molar ratio O_2/CO, the gas hourly space velocity (GHSV) and the inlet temperature on process performance of the reactor, in order to obtain high CO conversion and high selectivity with respect to the undesired H_2 oxidation. The model plays a key role in overcoming the issues of system design, by evaluating the temperature and the gas concentration profiles in the reactor. Simulation results showed the strong dependence of the overall performance upon the operating conditions examined.

1. Introduction

Fuel cell technology has been recently recognized as the most effective method to produce energy by both industrial R&D departments and academia. The Polymer Electrolyte Fuel Cell (PEFC) fuelled by hydrogen appears to be the key option for both transport and small scale combined heat and power applications, due to its compactness, modularity, higher conversion efficiencies and low emissions of noise and pollutants [1,2]. A growing interest for small stationary applications (in the 0.5–10 kW electrical output range) is developing; a large increase in the number of installed units in the world, as a decentralized power supply, grid support, peak shaving, power back-up or uninterruptible power supply (UPS), can be derived [3].

The absence of a hydrogen refuelling infrastructure and problems concerning hydrogen storage has led to the development of fuel processors able to convert available fuels (hydrocarbons and/or alcohols) into hydrogen rich reformate gas [4]. The choice of a suitable fuel processor and fuel, during the transition phase to a hydrogen economy, are key aspects to the successful implementation of direct-hydrogen fuel cell systems.

The key requirements for a fuel processor include rapid start-up, good dynamic-response to change in hydrogen demand, high fuel-conversion, small size and weight, simple design (construction and operation), stable performance for repeated start-up and shut-down cycles, maximum thermal integration, low cost and maintenance, high reliability and safety [5].

In small scale applications, natural gas remains the fuel most commonly employed for its wide availability and related infrastructure. For some niche markets, such as electricity production in remote sites, LPG could be an interesting optional fuel [6,7]. However, to utilize the reformate gas as a reactant for PEFC systems, clean-up steps must be considered to reduce the CO concentration to an acceptable level (10 ppm), since the fuel cell performance is progressively degraded by CO poisoning of the anode catalyst [8,9]. The reformate stream is purified using a two-stage process. The first stage is the water gas shift reaction, that reduces the carbon monoxide, increasing hydrogen content. The CO conversion is limited by equilibrium at the outlet temperature of the reactor. In the second stage the amount of carbon monoxide is further reduced using preferential oxidation reaction, which is the most compact of all the purification methods. Alternative technologies for the last clean-up step, such as Pressure Swing Adsorption (PSA) or Metal Separation Membranes, are not suitable for small scale applications, because high pressure requirements mandate the use of an additional compressor, and the need to re-humidify the hydrogen prior to use in fuel cells. Furthermore a desiccant must be used to adsorb water from the incoming wet gas stream in a PSA unit [10].

Because the PROX reaction is exothermic, the main drawback of a preferential oxidation reactor is complex temperature control system, in order to minimize parasitic hydrogen oxidation, since selectivity of oxygen to carbon monoxide deteriorates with

---

* Corresponding author. Tel.: +39 090 624 297; fax: +39 090 624 247.
E-mail address: francesco.cipiti@itae.cnr.it (F. Cipitì).

1385-8947/$ – see front matter © 2008 Elsevier B.V. All rights reserved.
doi:10.1016/j.cej.2008.09.004

Nomenclature

c_i	concentration of species i ($mol\,m^{-3}$)
c_i^0	inlet concentration of the species i ($mol\,m^{-3}$)
C_{pj}	heat capacity of air in the jacket ($J\,kg^{-1}\,K^{-1}$)
C_{pr}	heat capacity of gas in the reactor ($J\,kg^{-1}\,K^{-1}$)
$D_{i,eff}$	effective diffusion coefficient of species i ($m^2\,s^{-1}$)
D_{ij}	binary (species i, j) gas diffusion coefficients ($m^2\,s^{-1}$)
$D_{ij,eff}$	effective binary (species i, j) gas diffusion coefficients ($m^2\,s^{-1}$)
F_i	molar flow rate of the species i ($mol\,s^{-1}$)
h_i	molar enthalpy of the species i ($J\,mol^{-1}$)
ΔH_{CO}	enthalpy for the reaction of CO oxidation ($J\,mol^{-1}$)
ΔH_{H_2}	enthalpy for the reaction of H_2 oxidation ($m^2\,s^{-1}$)
k_f	thermal conductivity of the fluid ($W\,K^{-1}\,m^{-1}$)
k_{eff}	effective thermal conductivity in the reactor ($W\,K^{-1}\,m^{-1}$)
k_j	thermal conductivity in the jacket ($W\,K^{-1}\,m^{-1}$)
k_s	thermal conductivity of the solid ($W\,K^{-1}\,m^{-1}$)
k_w	thermal conductivity of the wall ($W\,K^{-1}\,m^{-1}$)
N_i	flux vector of species i ($mol\,m^{-2}\,s^{-1}$)
p_{O_2}	oxygen partial pressure (Pa)
q_j	heat flux vector in the jacket ($mol\,m^{-1}\,s^{-3}$)
q_r	heat flux vector in the reactor ($mol\,m^{-1}\,s^{-3}$)
Q	heat generation rate per unit volume of the catalyst bed ($J\,m^{-3}\,s^{-1}$)
r_{CO}	rate of CO oxidation ($mol\,kg_{cat}^{-1}\,s^{-1}$)
r_{H_2}	rate of H_2 oxidation ($mol\,kg_{cat}^{-1}\,s^{-1}$)
R_g	gas constant ($J\,mol^{-1}\,K^{-1}$)
R_i	net species' reaction term ($mol\,m^{-3}\,s^{-1}$)
T_j	jacket temperature (K)
T_r	reactor temperature (K)
T_0	inlet temperature of the reagent gas mixture (K)
T_j^0	inlet temperature of the air (K)
u_j	air velocity in the jacket ($m\,s^{-1}$)
u_r	velocity of the fluid in the reactor ($m\,s^{-1}$)
U_k	film coefficient ($W\,K^{-1}\,m^{-2}$)

Greek symbols

δ_w	thickness of the wall (m)
ε	void fraction of the catalyst bed
ρ_b	catalyst bulk density ($kg_{cat}\,m^{-3}$)
ρ_{gr}	gas density in the reactor ($kg\,m^{-3}$)
ρ_{gj}	gas density of the air in the interspace ($kg\,m^{-3}$)

Subscripts

cat	catalyst
eff	effective
f	fluid
g	gas
i	gas species, i = CO, O_2, CO_2, H_2, H_2O
in	inlet
j	jacket
r	reactor
s	solid
out	outlet

increasing operating temperatures [11]. The consequent oxidation of hydrogen causes a decrease in the process efficiency and increases water management issues. Multi-stage PROX reactors have been proposed [12–14], but complex hardware is required to control temperatures, using staged air injections along the catalyst bed. A single-stage PROX process could be an optimal solution, as reported by Echigo et al. [15]. It has been reported that Pt/Al_2O_3 catalysts showed higher CO removal performance than conventional Ru/Al_2O_3 catalysts in a temperature range 448–523 K [16–18].

During the last few years, research activity on the PROX reaction for small scale applications has focused on catalyst development/testing and reactor design optimization, in order to reduce the CO concentration to below 10 ppm to meet the fuel purity requirements for PEFC stacks.

Previous experimental tests with our 2 kWe LPG-based fuel processor (HYGen I) [19], designed for integration with a PEFC, showed some drawbacks in the CO preferential oxidation step: the CO content in the output of the reactor reached a CO level of 0.2% (dry basis). This content, incompatible with a PEFC system, showed the need of improving the prototype engineering, focusing on further efforts to achieve optimized design of the PROX subsystem, in terms of temperature control.

The objective of this study is to theoretically investigate the PROX kinetics by a modeling approach. A 2D steady state reactor model was developed, driving the design of a single-stage multi-tube reactor to overcome the system issues of heat management, considering Pt/Al_2O_3 catalysts (pellets form 3 mm × 3 mm). This geometrical configuration, with a cocurrent air in the cooling jacket (interspace), is used as a case study in developing a beta 5 kWe hydrogen generator [20–22]. Simulation studies on the influence of reactor geometrical parameters [23,24], comparing process performance with other two configurations (without a cooling jacket and with a countercurrent air flow in the interspace), showed that an optimal temperature control can be achieved using a configuration with a cocurrent air flow in the interspace. The model-based analysis make it possible to gain insight into the factors that limit PROX performance.

2. Reactor concept and design

The HYGen II system can generate hydrogen for Polymer Electrolyte Fuel Cells for small stationary applications. The prototype is able to convert light hydrocarbons (methane, LPG, butane) with a nominal hydrogen production of $5\,N\,m^3\,h^{-1}$ and a maximum hydrogen production of $8\,N\,m^3\,h^{-1}$. The net size (mm) of the fuel processor is 636 (width) × 868 (length) × 1350 (height).

The unit is based on three catalytic reaction steps: the Autothermal Reforming (ATR), the Intermediate Water Gas Shift (ITWS) and the preferential oxidation (PROX). The diagram of the integrated system is shown in Fig. 1; the processing unit is coupled with a heat exchanger, a static mixer, a water reservoir, manual/automatic valves, pressure regulators/transducers, flow meters and ancillaries.

The main issues in developing a commercially viable fuel processor are high energy efficiency, compact size and low cost for manufacturing and maintenance. Consequently, the system has been engineered, focusing on the design of every single component and the integration of the system, to minimize size, while improving thermal and mass transfer and system efficiency. The reformer uses a new design concept for integrating the CO preferential oxidation process and the heat transfer management into a suitable configuration, namely, a single-stage multi-tube reactor geometry. Hence the resulting unit is a single-stage multi-tube reactor, filled with pellet catalysts with a total volume of 4.38 l.

The single-stage multi-tube PROX reactor consists of 10 parallel and cylindrical tubes (Fig. 2): the product gas mixture from the previous water gas shift step enters into a static mixer where it is mixed with air and then reaches the heating zone, that consists of an inert bed heated by electrical heating elements only during start-up

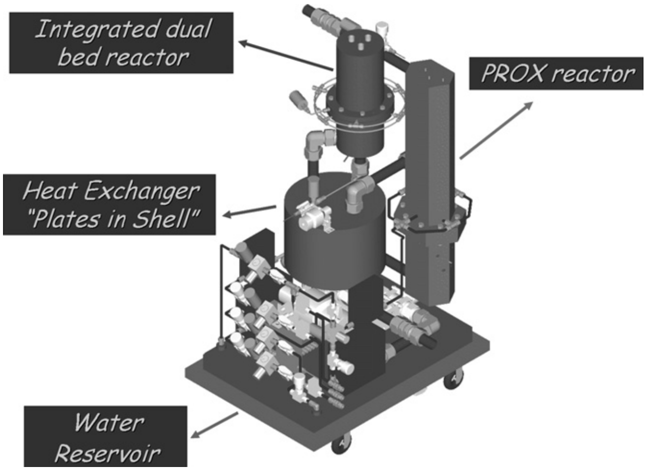

Fig. 1. Diagram of the 5 kWe hydrogen generator (HYGen II).

phase. Here the PROX reagent mixture is heated to reach the light-off temperature and then distributed uniformly into ten catalytic tubes. This geometry was designed to optimize flow distribution and improve heat transfer; the air required for the reaction is fed by means of a four injection satellite system, in order to uniformly distribute the air flow on the catalytic tubes. Then the air flows in the cooling jacket, making it possible to maintain the temperature reaction in an optimal operating range.

The reactor conditions, catalyst formulation and expected results have been derived from experimental results obtained on a laboratory scale [25,26] and on the previous HYGen I system [19,25,26]. From these results the range of operating conditions have been derived.

3. Multiphysics modelling simulation

3.1. Chemical kinetics

In a CO selective oxidation system, many reactions are taking place, with rates that depend strongly on the reactor geometrical parameters and on the operating conditions (molar ratio of CO/O_2, gas hourly space velocity and inlet reagent temperature). The five main reactions involved in a PROX reactor include [27–29]:

$$\text{CO oxidation}: \quad CO + \tfrac{1}{2}O_2 \rightarrow CO_2, \quad \Delta H_{(298)} = -283,000\,\text{J mol}^{-1} \tag{1}$$

$$H_2 \text{ oxidation}: \quad H_2 + \tfrac{1}{2}O_2 \rightarrow H_2O, \quad \Delta H_{(298)} = -242,000\,\text{J mol}^{-1} \tag{2}$$

Reverse water gas shift (RWGS) reaction :

$$CO_2 + H_2 \leftrightarrow CO + H_2O, \quad \Delta H_{(298)} = +41,100\,\text{J mol}^{-} \tag{3}$$

CO methanation :

$$CO + 3H_2 \rightarrow CH_4 + H_2O, \quad \Delta H_{(298)} = -206,300\,\text{J mol}^{-1} \tag{4}$$

CO_2 methanation :

$$CO_2 + 4H_2 \rightarrow CH_4 + 2H_2O, \quad \Delta H_{(298)} = -165,100\,\text{J mol}^{-1} \tag{5}$$

Some of these reactions have significantly low rates; to reduce the complexity in the developed model, only the reactions with significant rates are considered.

Since the main aim of the model is to investigate the process performance of the PROX reactor in the temperature range between 403 and 473 K, the previous model [23], based on the kinetics of the CO oxidation reaction, was implemented with the H_2 oxidation reaction. This temperate range is considered optimal to efficiently prevent the performance decrement of CO oxidation. It has been shown [11,30,31] that the carbon monoxide oxidation deteriorates at temperatures higher than 473 K, due to increasing hydrogen oxidation. Therefore, an investigation at temperatures higher than 473 K has been also carried out, to show that for the temperatures chosen the hydrogen oxidation is indeed unimportant, while increasing the temperature, it becomes significant. The CO conversion is slightly influenced by the reverse water gas shift reaction in the temperature range considered in steam excess, as the current investigation [27]; the relative reaction rate results insignificant for the purpose of the model. Moreover, the methanation reactions in

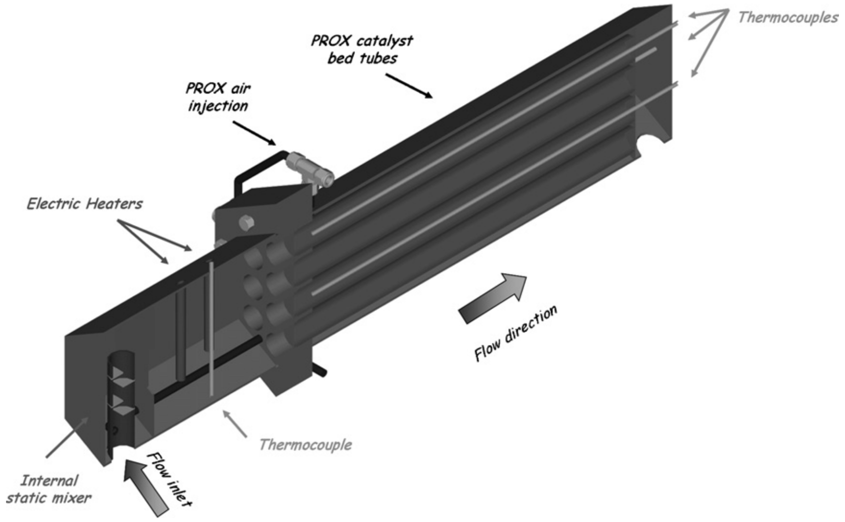

Fig. 2. Cut away view of the single-stage multi-tube PROX reactor.

the considered temperature range can be considered negligible, in accordance with Xu and Zhang [29].

Numerous kinetic modeling efforts for metal catalysts have been performed for CO preferential oxidation. Amphlett et al. [31] developed an approximate first order rate expression r_{CO} (mol s^{-1} kg$_{cat}{}^{-1}$) for platinum–alumina catalysts:

$$r_{CO} = k_{CO} \cdot c_{CO} \tag{6}$$

where c_{CO} (mol m^{-3}) denotes the CO concentration and k_{CO} (m^3 s^{-1} kg$_{cat}{}^{-1}$) the kinetic rate constant of the reaction, that can be expressed as follows:

$$k_{CO} = 0.0226\ \exp\left(-\frac{1000}{T_r}\right) \tag{7}$$

where T_r (K) denotes the reaction temperature.

Despite the kinetics and the rate expressions of the CO oxidation have been investigated in many studies, there are few papers that consider H_2 oxidation simultaneously with CO oxidation reaction. Maymo and Smith [32] reported an empirical power law expression for the H_2 oxidation rate r_{H_2} (mol s^{-1} kg$_{cat}{}^{-1}$) on platinum–alumina catalysts:

$$r_{H_2} = 6.19 \times 10^{-5}\ p_{O_2}{}^{0.804} \exp\left(-\frac{21.9 \times 10^3}{R_g \times T_r}\right) \tag{8}$$

with an activation energy of 21.9×10^3 J mol^{-1} and where p_{O_2} (Pa) denotes the oxygen partial pressure, R_g the gas constant (J mol^{-1} K^{-1}) and T_r (K) the reaction temperature. As shown, the H_2 oxidation reaction rate depends on the partial pressure of oxygen. In the model the oxygen partial pressure was correlated to its own concentration by using the ideal gas law.

3.2. Steady-state reactor model

The design of the single-stage multi-tube reactor was supported by a Computational Fluid Dynamics (CFD) approach. The design of a PROX reactor is the key aspect for the performance and efficiency of a compact hydrogen generator: weight and volume should be minimized and the heat management system optimized for different operating conditions. The design of any reactor requires a comprehensive investigation in order to understand the sources of performance limitations and identify possible means of process enhancement from the perspective of reactor configuration, catalyst formulation and process integration.

Based upon the above considerations, simulation studies aimed at describing the performance of the reactor, were performed by a mathematical model, based on energy and mass balances. The model is able to couple heat, mass transport and chemical reactions occurring in the reactor. The main aims of the mathematical model were to optimize the key operating conditions by a parametric analysis for different molar ratio of O_2/CO, gas hourly space velocity and inlet reagent temperature, and to evaluate the temperature distribution and gas concentration in the reactor, to gain insight into the design and operation of the PROX unit.

The mathematical simulations were achieved through the description of transport phenomena by Partial Differential Equations (PDEs), numerically solved through the Finite Element Methods (FEM), using a commercial software package Comsol Multiphysics.

The model simulation sequence is shown in Fig. 3.

First, the geometry of the reactor and the mesh map, related to the calculation tolerance, are defined. After introducing the catalyst and gas properties, the boundary conditions and initial values are assigned. The convergence of the solution determines the temperature and gas concentration distributions. In this model a state steady is assumed, so the time-dependent terms are dropped to simplify the analysis. Moreover, because the gas flow rate in the reactor is relatively low and the void fraction of the catalyst bed is high (ε = 0.35), a negligible pressure drop has been assumed: considering as reference case (O_2/CO = 2.0, GHSV = 4000 h^{-1}), a constant axial velocity (u_r of 0.76 m s^{-1}, Reynolds number = 857) in the reactor (volume flow rate/cross-section area of the reactor), and zero radial velocity were assumed: a constant axial velocity in the cooling jacket is also relatively low, the viscous effects can be ignored: the axial velocity (u_j of 0.044 m s^{-1}, Reynolds number = 340) in the cooling jacket (volume flow rate/cross-section area of the cooling jacket) and zero radial velocity were also assumed.

Gas density ρ_g (kg m^{-3}), binary gas diffusion coefficients D_{ij} (m^2 s^{-1}), thermal conductivity k$_f$ (W K^{-1} m^{-1}), heat capacity C_p (J kg^{-1} K^{-1}), and molar enthalpy of reaction ΔH (J mol^{-1}), depending on temperature and composition of the gas mixture [33], are determined from the properties and molar fractions of the individual species. In particular, heat capacity ($C_{p,i}$) and molar enthalpy (h_i) of the individual species i are determined using the polynomial format introduced by Gordon et al. [34].

Supported metal on porous materials presents different thermal conductivity with different loading and synthesis method. Empirical formulation has been used to evaluate the effective binary

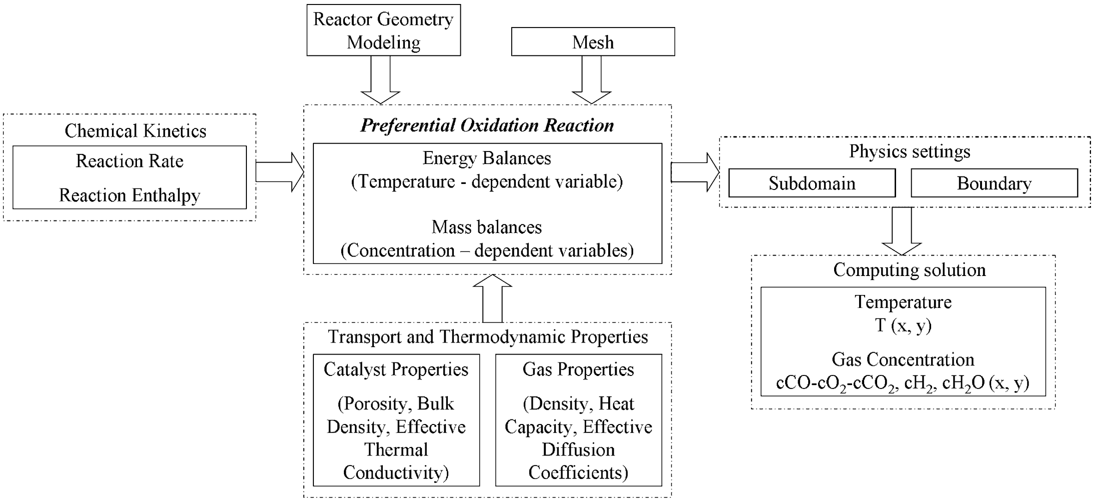

Fig. 3. Two-dimensional model simulation sequence to investigate process performance in the single-stage multi-tube PROX reactor.

Table 1
Equations used to describe the mass and heat transport phenomena in the reactor, and the heat transport phenomena in the interspace.

Transport phenomena equations		
Mass balances in the reactor	$\nabla\cdot(-D_{\mathrm{i,eff}}\nabla c_{\mathrm{i}}+c_{\mathrm{i}}u_{\mathrm{r}})=R_i$	(11)
Energy balances in the reactor	$\nabla\cdot(-k_{\mathrm{eff}}\nabla T_{\mathrm{r}}+\rho_{\mathrm{gr}}C_{\mathrm{pr}}T_{\mathrm{r}}u_{\mathrm{r}})=Q$	(12)
Energy balances in the interspace	$\nabla\cdot(-k_{\mathrm{j}}\nabla T_{\mathrm{j}}+\rho_{\mathrm{gj}}C_{\mathrm{pj}}T_{\mathrm{j}}u_{\mathrm{j}})=0$	(13)

Table 2
Reaction terms of the individual species.

Reaction terms	
$R_{\mathrm{CO}}=\rho_{\mathrm{b}}\cdot(-r_{\mathrm{CO}})$	(14)
$R_{\mathrm{O_2}}=\rho_{\mathrm{b}}\cdot(-0.5\cdot r_{\mathrm{CO}}-0.5\cdot r_{\mathrm{H_2}})$	(15)
$R_{\mathrm{CO_2}}=\rho_{\mathrm{b}}\cdot(+r_{\mathrm{CO}})$	(16)
$R_{\mathrm{H_2}}=\rho_{\mathrm{b}}\cdot(-r_{\mathrm{H_2}})$	(17)
$R_{\mathrm{H_2O}}=\rho_{\mathrm{b}}\cdot(+r_{\mathrm{H_2}})$	(18)

(species i, j) diffusion coefficients $D_{\mathrm{ij,eff}}$ ($\mathrm{m^2\,s^{-1}}$) [33,35,37] and the effective thermal conductivity k_{eff} ($\mathrm{W\,K^{-1}\,m^{-1}}$) [33,36] of the catalyst bed. Based on this approach, effective binary diffusion coefficients $D_{\mathrm{ij,eff}}$ ($\mathrm{m^2\,s^{-1}}$) are dependent on binary diffusion coefficient $D_{\mathrm{ij,f}}$ according to the following [35]:

$$D_{\mathrm{ij,eff}}=\frac{2\varepsilon}{3-\varepsilon}\cdot D_{\mathrm{ij,f}} \tag{9}$$

Since the effective thermal conductivity for packed beds is dependent on thermal conductivity of the solid k_{s} ($\mathrm{W\,K^{-1}\,m^{-1}}$), thermal conductivity of the fluid k_{f} ($\mathrm{W\,K^{-1}\,m^{-1}}$), and void fraction of the catalyst bed ε, can be expressed as [36]:

$$k_{\mathrm{eff}}=k_{\mathrm{s}}\cdot\left[1+\frac{3\varepsilon\cdot(1-k_{\mathrm{s}}/k_{\mathrm{f}})}{(1-\varepsilon)+k_{\mathrm{s}}/k_{\mathrm{f}}\cdot(2+\varepsilon)}\right] \tag{10}$$

The equations used to describe the mass and heat transport phenomena in the reactor, and the heat transport phenomena in the interspace, are reported in Table 1. Table 2 reports the reaction terms of the individual species i. The expression within the brackets in Eq. (11) represents the mass flux vector N_{i} ($\mathrm{mol\,m^{-2}\,s^{-1}}$) of species i; the first term describes the transport by diffusion, the second one represents the convective flux, namely:

$$N_{\mathrm{i}}=-D_{\mathrm{i,eff}}\nabla c_{\mathrm{i}}+c_{\mathrm{i}}u_{\mathrm{r}} \tag{19}$$

The heat generation rate per unit volume of the catalyst bed Q ($\mathrm{J\,m^{-3}\,s^{-1}}$) in Eq. (12), function of reaction rates and heats of reaction, can be expressed as follows:

$$Q=\rho_{\mathrm{b}}\cdot(-\Delta H_{\mathrm{CO}}\cdot r_{\mathrm{CO}}-\Delta H_{\mathrm{H_2}}\cdot r_{\mathrm{H_2}}) \tag{20}$$

The expression within the brackets in Eq. (12) represents the heat flux vector q_{r} ($\mathrm{mol\,m^{-1}\,s^{-3}}$); the first term describes the heat flux due to conduction, the second one represents the convective flux, namely:

$$q_{\mathrm{r}}=-k_{\mathrm{eff}}\nabla T_{\mathrm{r}}+\rho_{\mathrm{gr}}C_{pr}T_{\mathrm{r}}u_{\mathrm{r}} \tag{21}$$

In the Eq. (12) the conductive term accounts for the effective thermal conductivity of the catalyst bed, while the convective term accounts for the gas transport.

In order to calculate the temperature in the interspace, coupled with a thin film approximation for the interface reactor-interspace, a new temperature variable, T_{j}, is introduced for the interspace.

The expression within the brackets in Eq. (13) represents the heat flux vector in the cooling jacket q_{j} ($\mathrm{mol\,m^{-1}\,s^{-3}}$); the first term describes the transport by diffusion, the second one represents the convective flux, namely:

$$q_{\mathrm{j}}=-k_{\mathrm{j}}\nabla T_{\mathrm{j}}+\rho_{\mathrm{gj}}C_{\mathrm{pj}}T_{\mathrm{j}}u_{\mathrm{j}} \tag{22}$$

The single-stage multi-tube reactor consists of 10 cylindrical tubes, each one with an outside diameter of 38.1 mm, a thickness of 2.41 mm and a length of 480 mm. The distance between two close tubes is 5 mm, while between the centres of two close tubes is 43.1 mm. The tubes are placed in a parallel configuration along the flow direction and in a uniform distribution along the cross section of the flow, to improve heat management, as shown in Fig. 4.

For the purposes of this model a single cell unit, to represent a single catalytic tube, has been considered as a geometrical model (Fig. 5).

The model domains are the PROX reactor (single catalytic tube) and the interspace (cooling jacket). The PROX bed consists of the first 70 mm of inert bed, that acts as a flow distributor along the reactor's radius. An uniform air distribution in the interspace before the beginning of the PROX reaction was obtained.

The boundary conditions for the mass and energy balances in the reactor, and the energy balances in the interspace, are reported in Table 3. The film approximation condition at the wall that separates the reactor and the cooling jacket sets the flux as a function of the temperature difference across the wall.

Temperature and gas concentration along and across the reactor and the interspace were determined by the solution of the mass and heat balances, Table 1, in combination with initial and boundary conditions, Table 3, that define the mathematical model.

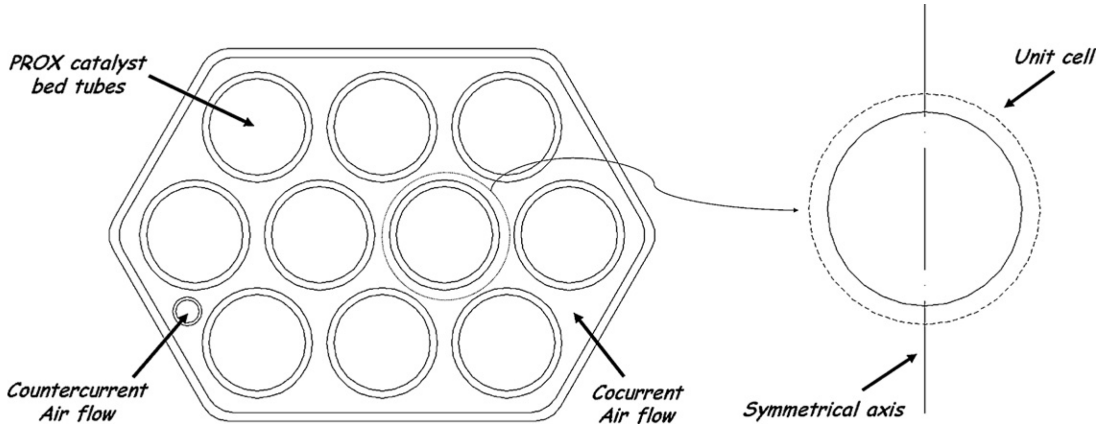

Fig. 4. Cross section of the single-stage multi-tube PROX reactor.

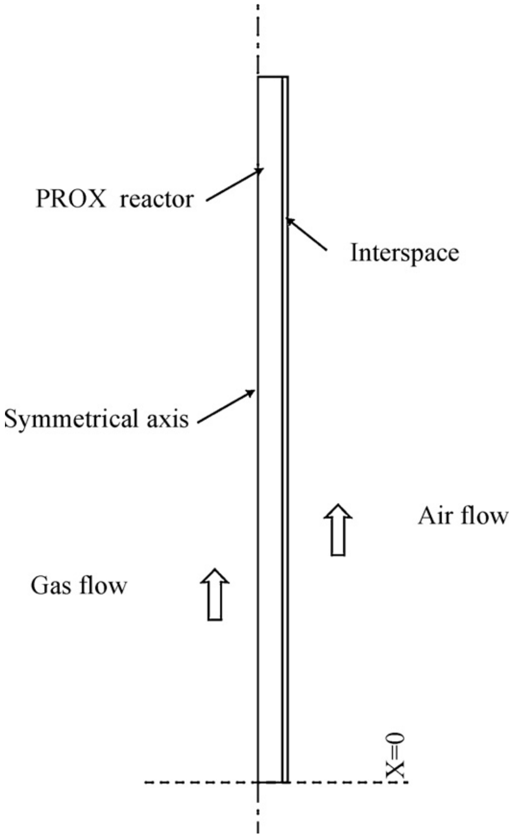

Fig. 5. Geometrical model in the mathematical simulations.

CO conversion and selectivity were calculated from the following equations as

$$CO_{\mathrm{conversion}} = \frac{F_{\mathrm{CO,in}} - F_{\mathrm{CO,out}}}{CO_{\mathrm{in}}} \times 100$$

$$CO_{\mathrm{selectivity}} = \frac{F_{\mathrm{CO,in}} - F_{\mathrm{CO,out}}}{2 \times (F_{\mathrm{O_2,,in}} - F_{\mathrm{O_2,out}})} \times 100$$

where F_{i} is the molar flow rate of the species i.

Table 3
Boundary conditions for the mass and heat transport balances in the reactor, and the heat balances in the cooling jacket.

Typology	Expression
Boundary conditions for the mass balances in the reactor	
Reactor inlet	$c_{\mathrm{i}} = c_{\mathrm{i}}^0$
Symmetry line and interface	$N_{\mathrm{i}} \cdot n = 0$
Reactor outlet	$N_{\mathrm{i}} \cdot n = c_{\mathrm{i}} u_{\mathrm{r}} \cdot n$
Boundary conditions for the energy balances in the reactor	
Reactor inlet	$T = T_0$
Symmetry line	$q_{\mathrm{r}} \cdot n = 0$
Reactor outlet	$q_{\mathrm{r}} \cdot n = \rho_{\mathrm{gr}} C_{pr} T_{\mathrm{r}} u_{\mathrm{r}} \cdot n$
Interface	$q_{\mathrm{r}} \cdot n = U_k (T_{\mathrm{r}} - T_{\mathrm{j}});\ \ U_k = k_{\mathrm{w}}/\delta_{\mathrm{w}};$
Boundary conditions for the energy balances in the cooling jacket	
Jacket inlet	$T_{\mathrm{j}} = T_{\mathrm{j}}^0$
Outer wall	$q_{\mathrm{j}} \cdot n = 0$
Jacket outlet	$q_{\mathrm{j}} \cdot n = \rho_{\mathrm{gj}} C_{pj} T_{\mathrm{j}} u_{\mathrm{j}} \cdot n$
Interface	$q_{\mathrm{j}} \cdot n = U_k (T_{\mathrm{j}} - T_{\mathrm{r}})$

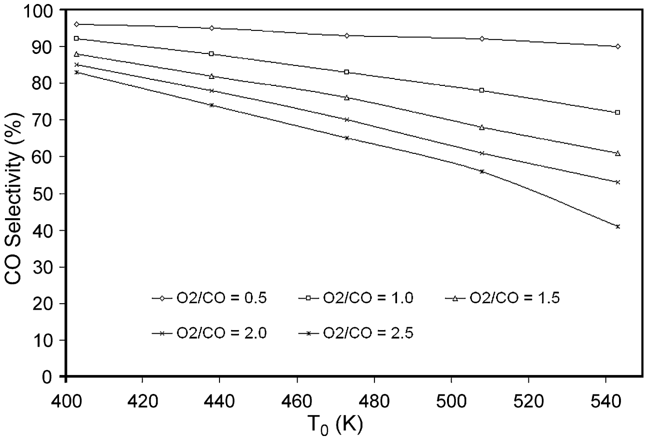

Fig. 6. CO selectivity at different inlet reagent temperature T_0 and O_2/CO molar ratio; GHSV = 4000 h^{-1}.

4. Simulation results and discussion

The predicted variation in the CO selectivity with respect to molar ratio O_2/CO and inlet reagent temperature under steady operating conditions at GHSV of 4000 h^{-1} is shown in Fig. 6. As expected, CO selectivity decreases, and consequently hydrogen consumption increases (not showed), by increasing temperature and O_2/CO molar ratio. Han et al. [38] report that, for high O_2/CO ratios, the reaction seems to saturate with the increase of O_2 pressure, while the selectivity decreases sharply, suggesting that the reac-

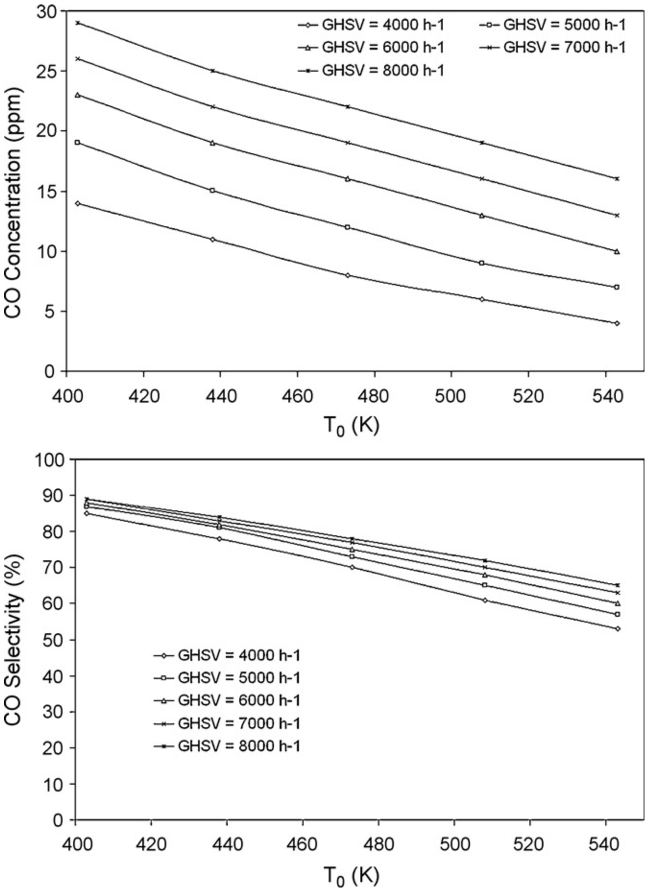

Fig. 7. CO concentration and CO selectivity at different inlet reagent temperature T_0 and GHSV;. O_2/CO = 2.

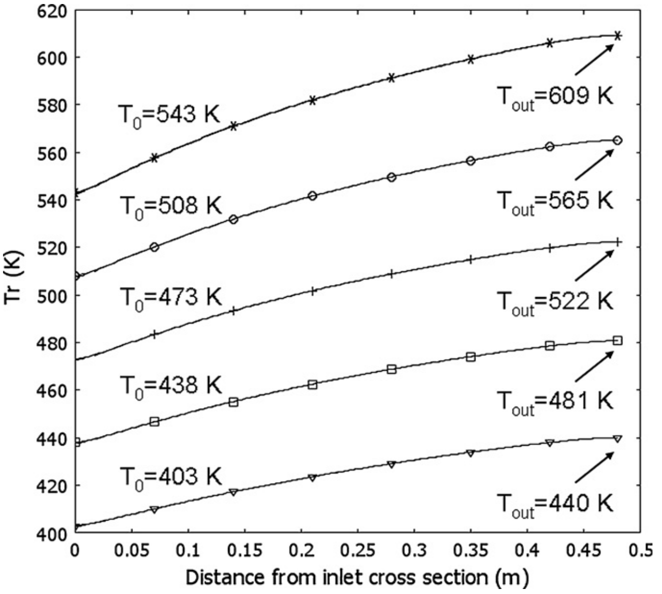

Fig. 8. Temperature profiles through the length of the reactor at different inlet reagent temperatures T_0—base case: $O_2/CO = 2$, GHSV = 4000 h^{-1}.

tion mechanism is altered for high O_2/CO values. This effect can be related to the reduced CO adsorption energy on the oxidized catalytic surface as the temperature increases. At higher temperatures, the surface coverage of CO decreases, allowing for hydrogen adsorption and oxidation [30].

At low temperatures, the selectivity remains high until the CO is virtually depleted and then the remaining oxygen reacts with hydrogen, while low selectivity at high temperature can be due to increased H_2 oxidation. Since oxygen is the limiting reactant, the reduction of CO selectivity indicates that the oxidation rate of hydrogen becomes significant at higher temperatures. The oxygen level is an important factor in PROX operation: excess oxygen can imply high hydrogen consumption, while a low oxygen concentration in the stream can result in a poor CO abatement. Considering that the CO content at a previous water gas shift reaction step exit can fluctuate incidentally during the transient operation, a value of molar ratio O_2/CO of 2 seems to represent a good compromise.

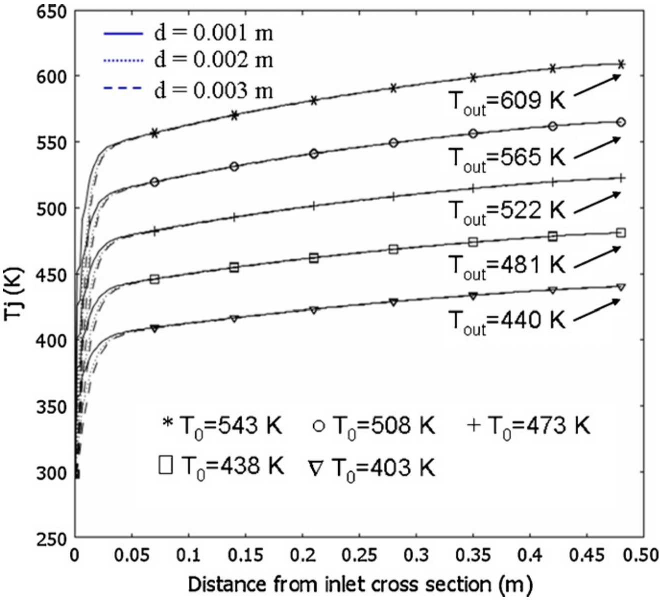

Fig. 9. Temperature profiles through the length of the interspace, at different distances (d) from the wall and at different inlet reagent temperatures T_0—base case: $O_2/CO = 2$, GHSV = 4000 h^{-1}.

Fig. 7 shows the variations of CO concentration and CO selectivity as a function of inlet temperature and GHSV of the feed gas with O_2/CO of 2. An optimal GHSV, in order to obtain a reactor as compact as possible, with an acceptable CO exit concentrations of about 10 ppm, can be predicted at GHSV of 4000 h^{-1}, with CO conversion (not showed) and CO selectivity higher than 80% in the inlet temperature range between 433 and 473 K.

Fig. 8 shows for the case base identified ($O_2/CO = 2$, GHSV = 4000 h^{-1}), that the temperature in cross sections along the length of the reactor is almost fully uniform at any fixed inlet reagent temperature. Hence, the heat used to preheat the incoming air among the catalyst tubes does not cause a temperature gradient at different distances from the symmetry axis, allowing for constant catalyst performance. Moreover, the temperature along the length of the reactor increases up to a maximum value for all inlet reagent temperatures. For higher inlet temperature, the differences 37 K (T_0 = 403 K), 43 K (T_0 = 408 K), 49 K (T_0 = 473 K), 57 K (T_0 = 508 K), 66 K (T_0 = 543 K) between the maximum temperature and the inlet temperature increase since the exothermic effects of the reaction become more relevant. The temperature increase

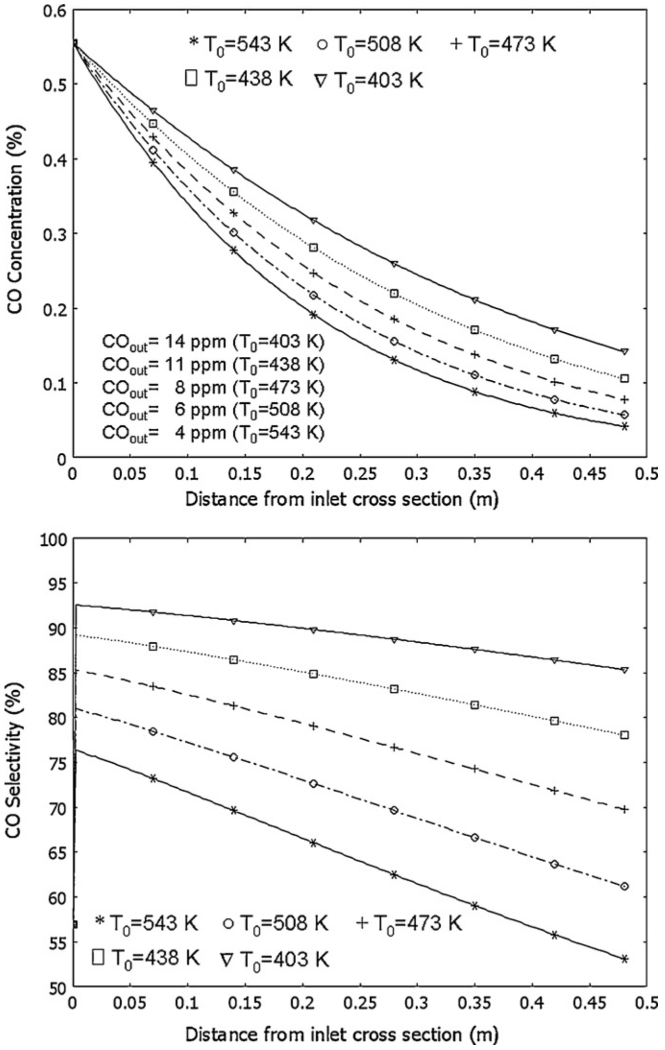

Fig. 10. CO concentration and CO selectivity distribution through the length of the reactor, at different inlet reagent temperature T_0—base case: $O_2/CO = 2$, GHSV = 4000 h^{-1}.

is more rapid in the first half of the catalyst bed, more evident increasing the inlet temperature, indicating that the heat exchange to control reactor temperature should be in the incoming reagents side. These results suggest that the cocurrent air flow solution can be optimal from the temperature control point of view.

Fig. 9 shows the related temperature change in the cooling jacket. The almost overlapping temperature curves (for three different distances from the wall—0.001 m, 0.002 m and 0.003 m) at any fixed inlet temperature, imply that the temperature in cross sections (ring-shape) along the length of the interspace is almost fully uniform; the air temperature increases rapidly near the front face of the jacket (3 cm from the beginning of the inlet cross section), and then increases gradually, suggesting that the heat transfer from the catalyst bed to the air flow occurs mainly near the front face. Moreover, the outlet air and the outlet product gas in the catalyst reactor reach the same temperature, confirming that the main heat transfer zone is located near the front face of the jacket.

The CO concentrations and CO selectivity profiles along the reactor center for different inlet reagent temperatures are presented in Fig. 10 for the case base identified (O_2/CO = 2, GHSV = 4000 h^{-1}).

Results show that CO is continuously consumed when the gas mixture passes along the catalyst tube. The concentration curves indicate that the consumption rates of CO are faster in the front face of the reactor, and lower in the rear part, in accordance with the temperature profiles. The predicted CO consumptions (outlet CO concentrations between 4 and 14 ppm) suggest that the reactor length is long enough to reach a good conversion level. Moreover, while CO conversion (not showed) increase with the reactor temperature, CO selectivity decreases, due to the undesired H_2 oxidation.

5. Conclusions

A comprehensive investigation by a modeling approach, in order to explore reactor geometrical configuration and the effects of the main operating parameters on CO preferential oxidation performance has been carried out. The reactor configuration is a single-stage multi-tube geometry with a cocurrent air flow in the cooling jacket. The study considered heat and mass transport phenomena associated with two main simultaneous chemical kinetic reactions in the reactor: CO oxidation and H_2 oxidation.

Simulation results showed that the reactor performance depends strongly on the O_2/CO molar ratio, GHSV and inlet temperature. Sufficient carbon monoxide conversion and temperature control in the preferential oxidation reactor can be achieved with the following optimal operating conditions: a molar ratio O_2/CO of 2, a GHSV of 4000 h^{-1} and an inlet reagent temperature in the range 435–475 K.

References

[1] A. Heinzel, B. Vogel, P. Hübner, Reforming of natural gas—hydrogen generation for small scale stationary fuel fell systems, J. Power Sources 105 (2) (2002) 202–207.

[2] K.A. Adamson, G. Crawley, D. Jollie, Fuel Cell Today 2006 Worldwide Survey, 2006 (accessed November 1, 2007) www.fuelcelltoday.com.

[3] K.A. Adamson, Fuel Cell Today Market Survey: Small Stationary Applications 2006, 2006 (accessed November 1, 2007) www.fuelcelltoday.com.

[4] F. Joensen, J.R. Rosstrup-Nielsen, Conversion of hydrocarbons and alcohols for fuel cells, J. Power Source 105 (2) (2002) 195–201.

[5] S. Ahmed, M. Krumpelt, Hydrogen from hydrocarbon fuels for fuel cells, Int. J. Hydrogen Energy 26 (4) (2001) 291–301.

[6] T. Rampe, A. Heinzel, B. Vogel, Hydrogen generation from biogenic and fossil fuels by autothermal reforming, J. Power Sources 86 (1/2) (2000) 536–541.

[7] A.K. Avci, Z. Ilsen Onsan, D.L. Trimm, On-board fuel conversion for hydrogen fuel cells: comparison of different fuels by computer simulations, Appl. Catal. A: Gen. 216 (1/2) (2001) 243–256.

[8] J.D. Moon, K. Sreekumar, S.D. Lee, B.G. Lee, K.H. Sik, Studies on gasoline fuel processor system for fuel-cell powered vehicles application, Appl. Catal. A: Gen. 215 (1–2) (2001) 1–9.

[9] Z.G. Zhang, G. Xu, X. Chen, K. Honda, T. Yoshida, Process development of hydrogenous gas production for PEFC from biogas, F. Process. Technol. 85 (8–10) (2004) 1213–1229.

[10] Hydrogen Fuel Cell Engines and Related Technologies, College of the Desert and SunLite Transit Agency, Module 2: Hydrogen Use, 2001 (accessed September 1, 2005) http://www.eere.energy.gov.

[11] J.M. Zalc, D.G. Loffler, Fuel processing for PEM fuel cells: transport and kinetic issues of system design, J. Power Sources 111 (1) (2002) 58–64.

[12] C.D. Dudfield, R. Chen, P.L. Adcock, A compact CO selective oxidation reactor for solid polymer fuel cell powered vehicle application, J. Power Sources 86 (1/2) (2000) 214–222.

[13] M.A. Inbody, R.L. Borup, J.I. Tafoya, Transient PROX carbon monoxide measurement, in: Control and Optimization Abstracts of 2002 Fuel Cell Seminar, Palm Springs, CA, USA, 2002, pp. 94–97.

[14] S.H. Lee, J. Han, K.Y. Lee, Development of 10-kWe preferential oxidation system for fuel cell vehicles, J. Power Sources 109 (2) (2002) 394–402.

[15] M. Echigo, N. Shinke, S. Takami, T. Tabata, Performance of a natural fuel processor for residential PEFC system using a novel CO preferential oxidation catalyst, J. Power Sources 132 (1–2) (2004) 29–35.

[16] S. Kawatsu, Advanced PEFC development for fuel cell powered vehicles, J. Power Sources 71 (1/2) (1998) 150–155.

[17] D.J. Suh, C. Kwak, J.H. Kim, S.M. Kwon, T.J. Park, Removal of carbon monoxide from hydrogen-rich fuels by selective low-temperature oxidation over base metal added platinum catalysts, J. Power Sources 142 (2005) 70–74.

[18] M. Echigo, T. Tabata, A study of CO removal on an activated Ru catalyst for polymer electrolyte fuel cell applications, Appl. Catal. A 251 (2) (2003) 157–166.

[19] F. Cipitì, V. Recupero, L. Pino, A. Vita, M. Laganà, Experimental analysis of a 2 kWe LPG based fuel processor for PEFC, J. Power Sources 157 (2) (2005) 914–920.

[20] F. Cipitì, V. Recupero, L. Pino, A. Vita, M. Laganà, 5 kWe LPG hydrogen generator for PEFC: momentum-based modelling of an autothermal reformer, ASME J. Fuel Cell Sci. Technol. 4 (2) (2007) 210–218.

[21] F. Cipitì, L. Pino, A. Vita, M. Laganà, V. Recupero, Performance of a 5 kWe fuel processor for polymer electrolyte fuel cells, in: Proceedings of the HYSYDAYS—2nd World Congress of Young Scientists on Hydrogen Energy Systems, Torino, Italy (CD-Rom), 2007.

[22] V. Recupero, F. Cipitì, L. Pino, A. Vita, M. Laganà, Stability tests of a 5 kWeq LPG hydrogen generator for PEFC, in: Abstracts of 2007 Fuel Cell Seminar & Exposition, San Antonio, TX, USA (CD-Rom), 2007.

[23] F. Cipitì, L. Pino, A. Vita, M. Laganà, V. Recupero, Model-based investigation of a CO preferential oxidation reactor for polymer electrolyte fuel cell system, Int. J. Hydrogen Energy 32 (16) (2007) 4040–4051.

[24] F. Cipitì, L. Pino, A. Vita, M. Laganà, V. Recupero, Model-based analysis of reactor geometrical configuration on CO preferential oxidation performance, in: Proceedings of the World Hydrogen Technologies Convention 2007, Montecatini Terme, Italy (CD-Rom), 2007.

[25] V. Recupero, L. Pino, A. Vita, F. Cipitì, M. Cordaro, M. Laganà, Development of a LPG fuel processor for PEFC systems: laboratory scale evaluation of autothermal reforming and preferential oxidation subunits, Int. J. Hydrogen Energy 30 (9) (2005) 963–971.

[26] L. Pino, A. Vita, F. Cipitì, M. Laganà, V. Recupero, Performance of Pt/CeO_2 catalyst for propane oxidative steam reforming, Appl. Catal. A 306 (2006) 68–77.

[27] Y. Choi, H.G. Stenger, Kinetic, simulation and insights for CO selective oxidation in fuel cell applications, J. Power Sources 129 (2) (2004) 246–254.

[28] X. Ouyang, R.S. Besser, Effect of reactor heat transfer limitations on CO preferential oxidation, J. Power Sources 141 (1) (2005) 39–46.

[29] G. Xu, Z.G. Zhang, Preferential CO oxidation on Ru/Al_2O_3 catalyst: an investigation by considering the simultaneously involved methanation, J. Power Sources 157 (1) (2006) 64–77.

[30] M.J. Kahlich, H.A. Gasteige, R.J. Behm, Kinetics of the selective CO oxidation in H_2-rich gas on Pt/Al_2O_3, J. Catal. 171 (1) (1997) 93–105.

[31] J.C. Amphlett, R.F. Mann, B.A. Peppley, On board hydrogen purification for steam reformation/PEM fuel cell vehicle power plants, Int. J. Hydrogen Energy 21 (8) (1996) 673–678.

[32] A. Maymo, J.M. Smith, Catalytic oxidation of hydrogen-intrapellet heat and mass transfer, AICHE J. 12 (5) (1996) 845–854.

[33] R.C. Reid, J.M. Prausnitz, B.E. Poling, The Properties of Gases and Liquids, fourth edition, McGraw-Hill, 1987.

[34] B.J. McBride, S. Gordon, M.A. Reno, Coefficients for calculating thermodynamic and transport properties of individual species, NASA Report TM-4513, 1993.

[35] M. Kaviany, Principles of Heat Transfer in Porous Media, Springer-Verlag, 1991, p. 349.

[36] M. Kaviany, Principles of Heat Transfer in Porous Media, Springer-Verlag, 1991, p. 125.

[37] G.F. Froment, K.B. Bischoff, Chemical Reactor Analysis and Design, second edition, Wiley, New York, 1990.

[38] Y.F. Han, M.J. Kahlich, M. Kime, R.J. Behm, Kinetic study of the selective CO oxidation in H_2-rich gas on a Ru/γ-Al_2O_3 catalyst, Phys. Chem. Chem. Phys. 4 (2002) 389–397.